INORGANIC CHEMISTRY FRONTIERS

REVIEW

View Article Online
View Journal | View Issue

Cite this: *Inorg. Chem. Front.*, 2025, **12**, 2182

Selenoborates: a latent structure resource for infrared functional crystal materials

Yihan Yun,[a,b] Abudukadi Tudi,[a,b] Zhihua Yang,[a,b] Guangmao Li *[a,b] and Shilie Pan *[a,b]

Received 1st November 2024,
Accepted 16th January 2025

DOI: 10.1039/d4qi02770a

rsc.li/frontiers-inorganic

Optoelectronic functional crystal materials are crucial components in laser systems and could be applied as polarized light converters, modulators, photorefractive devices, window materials *etc*. Borates and chalcogenides are well-established sources of ultraviolet (UV) and infrared (IR) optoelectronic functional crystal materials. The selenoborate system combines the structural diversity of borates with the extensive optical transmission range of metal selenides, showing potential as IR functional materials. However, research on selenoborates remains limited. This review aims to stimulate further research into IR optoelectronic functional crystal materials within the selenoborate system. First, this work offers a comprehensive review of all selenoborates (21) reported to date, categorizing them according to their structural motifs from zero to three dimensions. Second, the unique synthesis methods of selenoborates are summarized. Additionally, first-principles calculations are utilized to analyze the bandgaps and nonlinear optical (NLO) properties of these materials. As a result, it is concluded that selenoborates possess considerable potential for further investigation as IR functional materials, especially in terms of the structures and properties regulated by excellent microstructural groups.

1. Introduction

The development of laser technology is highly regarded by scientific researchers, and has propelled rapid advancements in various fields, such as industrial manufacturing, medicine, communication and the military.[1–3] Optoelectronic functional crystal materials are essential components of laser technology, with applications extending to laser crystals, modulators, frequency multipliers, and optical window materials.[4–7] Currently, prevalent systems of optoelectronic functional crystal materials include borates, phosphates, carbonates, nitrates, chalcogenides, phosphides and so on.[8–24]

Exploration of suitable systems may promote the development of target materials in this field. Since the determination of the first borate single crystal structure, $Be_2BO_3(OH)$, in 1931, a growing number of well-characterized borates have been discovered and utilized as ultraviolet (UV) and deep-ultraviolet (DUV) optoelectronic functional crystals. Notable examples include $KBe_2BO_3F_2$ (KBBF), β-BaB_2O_4 (β-BBO) and LiB_3O_5 (LBO).[25–36] Recently, Pan's group advanced research in the fluoroborate system, reaching significant milestones in DUV nonlinear optical (NLO) crystals. Phosphate crystals such as KH_2PO_4 (KDP) and $KTiOPO_4$ (KTP) have been employed as optoelectronic functional crystal materials in the visible to near-infrared (IR) region. Meanwhile, chalcopyrite-type chalcogenides $AgGaS_2$ (AGS) and $AgGaSe_2$ (AGSe) have been widely used as commercial optoelectronic functional crystal materials in the mid- to far-IR region.[37–41] Combining the advantages of borates and chalcogenides, thioborates possess structural diversity and suitable transmission ranges. The exploration of the thioborate system by the Pan and Mao groups has led to the discovery of high-performance IR optoelectronic functional materials, such as BaB_2S_4 and $LaBS_3$.[42–55] Thus, exploring and developing specific systems are crucial for discovering new high-performance materials.

Metal chalcogenides represent one of the most extensively studied families for obtaining IR optoelectronic functional crystal materials, demonstrating significant importance in both civil and military fields.[56–65] Compared to isostructural sulfides, metal selenides exhibit wider IR transmittance and larger SHG responses.[66–68] Besides, they have lower melting points in most cases, which is beneficial for crystal growth. With the expectation of obtaining high-performance IR functional crystals, selenoborates derived from thioborates naturally attract our attention. Up to now, there are few cases of selenoborates, most of which are reported by Krebs from the 1990s to the 2000s. In the selenoborate system, [BSe_3] and

[a]*Research Center for Crystal Materials; CAS Key Laboratory of Functional Materials and Devices for Special Environments; Xinjiang Technical Institute of Physics & Chemistry, CAS, 40-1 South Beijing Road, Urumqi 830011, China.*
E-mail: slpan@ms.xjb.ac.cn, ligm@ms.xjb.ac.cn
[b]*Center of Materials Science and Optoelectronics Engineering, University of Chinese Academy of Sciences, Beijing 100049, China*

[BSe_4] are the basic structural units, which could be interconnected to form zeolitic [B_7Se_{13}] and hypertetrahedral [$B_{10}Se_{20}$] units.[69] This phenomenon indicates greater space for discovering structural diversity in the selenoborate system (Fig. 1).

In this paper, the calculated microstructural performances of related units indicate that the vibrational frequencies of [BSe_3] and [BSe_4] show obvious shifts to lower absorption energies (maximum 725 cm^{-1}) in comparison with those of [BS_n] (n = 3, 4) (maximum 911 cm^{-1}), which indicates that selenoborates have a long IR absorption edge (725 cm^{-1}, >12 μm) that covers two atmospheric transparent windows (3–5 and 8–12 μm). In addition, [BSe_3] demonstrates the highest polarizability anisotropy and hyperpolarizability (Fig. 2) among related units (BQ_x (Q = S, Se, x = 3, 4), GaQ_4 (Q = S, Se), ASe_4 (A = Zn, As, Sn, Ge, Si, Al)). The highest polarizability anisotropy and hyperpolarizability values suggest the ability of selenoborates demonstrating large birefringence and SHG responses. The above results theoretically indicate that selenoborates may be potential IR functional materials.

Besides, we present a comprehensive structural review of the 21 reported selenoborates cataloged in the Inorganic Crystal Structure Database (ICSD) with version 5.2.0 being the latest release as ICSD-2024/01. These selenoborates are classified into four categories based on the polymerization degree of their anionic units (Table 1). We analysed their structural characteristics and found that the majority of these selenoborates were formed from [BSe_4], with only three consisting of [BSe_3]. This is different from thioborates, among which most of them are composed of [BS_3]. Furthermore, we summarized the synthesis methods employed for these selenoborates. The challenge of B–Si exchange occurring at temperatures above 300–400 °C is addressed by using carbon-coated silica tubes and glassy carbon crucibles during the synthesis process. In addition, we calculated the bandgaps and SHG coefficients of selected selenoborates using density functional theory (DFT) calculations to investigate the properties of selenoborate system. The paper also discussed future directions for enhancing the structural diversity and optimizing the second-order nonlinearity of selenoborates, aiming at advancing the development of these material systems.

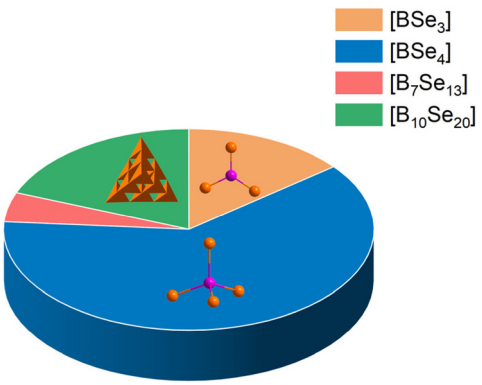

Fig. 1 The building units of reported selenoborates (based on the ICSD).

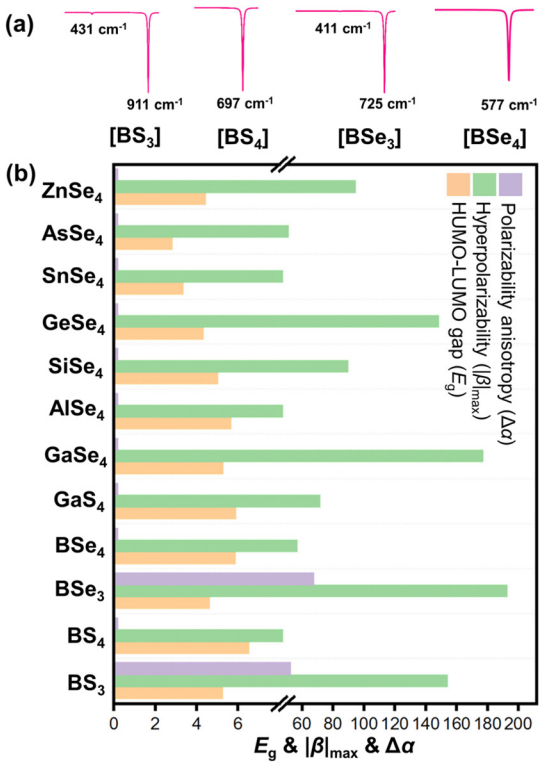

Fig. 2 The comparison of the microstructural performances of related units. (a) Vibrational data; (b) Polarizability anisotropy, hyperpolarizability and HUMO-LUMO gap.

2. Syntheses

At present, the discovery of selenoborates remains limited, primarily due to the difficulty of their synthesis. This section provides an overview of the commonly used synthesis methods, the prevailing difficulties in this field and distinctive synthesis methods for reference. Similar to that of thioborates, most selenoborates are synthesized *via* solid-state reactions involving metal selenides, amorphous boron, and selenium as raw materials. These reactions are typically conducted in evacuated carbon-coated silica tubes under precisely controlled conditions, often at temperatures ranging from 600 to 950 °C. However, obtaining highly pure selenoborates with well-defined structures remains a formidable challenge. This difficulty is largely attributed to the high reactivity of boron chalcogenides with various container materials at elevated temperatures. In particular, the widely employed fused silica tubes prove vulnerable to the corrosive effects of boron selenide when temperatures surpass the threshold of 300–400 °C. This interaction prompts the exchange of boron with silicon, instigating the formation of selenosilicate.

To overcome these challenges and procure pure selenoborate samples, two distinctive methods could be employed:

Table 1 Structural information regarding reported selenoborates based on ICSD

Formula	Crystal system	Point group	Space group	Symmetry	Lattice parameters (Å, °)	Building unit	Ref.
Zero dimensional							
Tl_3BSe_3	Monoclinic	2/*m*	$P2_1/m$ (No. 11)	CS	a = 5.547(2), b = 10.099(3), c = 6.852(2), β = 97.59(3)	BSe_3	70
$Ba_7(BSe_3)_4Se$	Monoclinic	2/*m*	$C2/c$ (No. 15)	CS	a = 10.513(2), b = 25.021(5), c = 10.513(2), β = 90.10(3)	BSe_3	71
$Ba_3(BSe_3)(SbSe_3)$	Hexagonal	$\bar{6}m$	$P\bar{6}2m$ (No. 189)	NCS	a = 17.720(4), c = 11.251(3)	BSe_3	73
$Li_{6-2x}Sr_{2+x}B_{10}Se_{20}$ ($x \approx 0.7$)	Tetragonal	4/*m*	$I4_1/a$ (No. 88)	CS	a = 14.735(6), c = 14.145(12)	$B_{10}Se_{20}$	72
One dimensional							
$Na_2B_2Se_7$	Monoclinic	2/*m*	$C2/c$ (No. 15)	CS	a = 11.863(4), b = 6.703(2), c = 13.811(2), β = 109.41(2)	BSe_4	75
$K_2B_2Se_7$	Monoclinic	2/*m*	$C2/c$ (No. 15)	CS	a = 12.092(4), b = 7.054(2), c = 13.991(5), β = 107.79(3)	BSe_4	75
$CsBSe_3$	Monoclinic	2/*m*	$P2_1/c$ (No. 14)	CS	a = 7.570(2), b = 12.791(4), c = 6.171(2), β = 107.09(2)	BSe_4	74
$RbBSe_3$	Monoclinic	2/*m*	$P2_1/c$ (No. 14)	CS	a = 7.2789(15), b = 12.385(3), c = 6.1690(12), β = 105.67(3)	BSe_4	74
$TlBSe_3$	Monoclinic	*m*	*Cc* (No. 9)	NCS	a = 6.1662(12), b = 12.109(2), c = 7.0311(14), β = 113.88(3)	BSe_4	74
$Cs_3B_3Se_{10}$	Triclinic	$\bar{1}$	$P\bar{1}$ (N0. 2)	CS	a = 7.5831(15), b = 8.4643(17), c = 15.276(3) α = 107.03(3), β = 89.29(3), γ = 101.19(3)	BSe_4	76
$Tl_3B_3Se_{10}$	Triclinic	$\bar{1}$	$P\bar{1}$ (N0. 2)	CS	a = 7.0989(14), b = 8.0724(16), c = 14.545(3) α = 105.24(3), β = 95.82(3), γ = 92.79(3)	BSe_4	76
$Tl_2B_2Se_7$	Monoclinic	2/*m*	$C2/c$ (No. 15)	CS	a = 11.878(2), b = 7.0909(14), c = 13.998(3), β = 108.37(3)	BSe_4	76
$Rb_2B_2Se_7$	Monoclinic	2/*m*	$C2/c$ (No. 15)	CS	a = 12.414(3), b = 7.314(2), c = 14.092(3), β = 90107.30(3)	BSe_4	76
Two dimensional							
$Ba_2B_4Se_{13}$	Monoclinic	2/*m*	$P2_1/c$ (No. 14)	CS	a = 12.790(3), b = 11.560(2), c = 12.862(3), β = 103.22(3)	BSe_4	77
BaB_2Se_6	Orthorhombic	*mmm*	*Cmca* (No. 64)	CS	a = 11.326(2), b = 7.6587(15), c = 10.315(2)	BSe_4	77
$Li_{6-x}Cs_xB_{10}Se_{18}$ ($x \approx 1$)	Tetragonal	4/*mmm*	$I4_1/amd$ (No. 141)	CS	a = 10.0285(14), b = 10.0285(14), c = 27.743(6)	$B_{10}Se_{20}$	78
Three dimensional							
$CuBSe_2$	Tetragonal	$I\bar{4}2m$	$I\bar{4}2d$ (No. 122)	NCS	a = 5.539, b = 5.539, c = 10.734	BSe_4	79
$Li_2B_2Se_5$	Monoclinic	2/*m*	$C2/c$ (No. 15)	CS	a = 10.616(2), b = 5.3181(11), c = 12.382(3), β = 109.96(3)	BSe_4	81
$Na_6B_{10}Se_{18}$	Tetragonal	4/*mmm*	$I4_1/acd$ (No. 142)	CS	a = 15.128(2), b = 15.128(2), c = 27.955(6)	$B_{10}Se_{20}$	83
$Li_{6+2x}[B_{10}Se_{18}]Se_x$ ($x \approx 2$)	Monoclinic	2/*m*	$C2/c$ (No. 15)	CS	a = 17.411(1), b = 21.900(1), c = 17.820(1), β = 101.6(1)	$B_{10}Se_{20}$	84
$Li_7B_7Se_{15}$	Tetragonal	4/*mmm*	$P4_2/nbc$ (No. 133)	CS	a = 11.4107(4), c = = 16.4251(5)	B_7Se_{13}	82

(i) Coating the inner surfaces of the containers with glassy carbon:

The silica tubes are coated on their inner surface with glassy carbon, which can be manufactured by slowly rotating the ampoule filled with acetone vapour helically through the flame of an oxygen–hydrogen welding torch at about 1300 K.

(ii) Utilizing glassy carbon or boron nitride crucibles:

The crucibles, fashioned from glassy carbon or boron nitride, measuring 100 mm in length with cap/outer/inner diameters of 18/12/5 mm, are meticulously sealed with a screw cap. These crucibles function as robust sample containers that are resistant to the corrosive tendencies of selenoborate synthesis.

After these preparatory measures, the crucibles are strategically positioned within outer silica tubes, whose inner walls are lined with glassy carbon. Then the tubes are fused. Given the air and moisture sensitivity inherent in selenoborates, all manipulations are conducted within a controlled environment – a glove box saturated with dry argon. To further shield against oxidation, the synthesized materials are placed within steel or tantalum ampoules, which are enveloped by an argon atmosphere. These ampoules are then carefully placed inside evacuated silica tubes, creating a multi-layered protective system. In addition to solid-state reactions, $CuBSe_2$ was synthesized *via* solvothermal methods. The reagents were placed in a 50 mL Teflon-lined autoclave filled to 80% with anhydrous diethylenetriamine, sealed and heated at 180 °C for 36 hours before cooling naturally to room temperature. Despite notable progress in synthesis techniques, obtaining highly pure selenoborates remains a formidable task. One possible method is to perform various purifications on the initially synthesized sample, such as cleaning, recrystallization, and so on. Successful cases are rare, underscoring the intricate nature of this process. With continuous exploration, progress is expected in the synthesis of selenoborates.

3. Structural classification

A comprehensive review of the structural motifs of all known selenoborates based on the ICSD database was summarized. Similar to thioborates, selenoborates are characterized by two fundamental building units: the trigonal-planar $[BSe_3]$ unit and the tetrahedral $[BSe_4]$ unit (Fig. 3a and b). These units can interconnect to form a variety of structures. Additionally, multiple $[BSe_4]$ units could be connected with each other to form the $[B_7Se_{13}]$ unit and the supertetrahedral $[B_{10}Se_{20}]$. Structures containing $[BSe_3]$ units are predominantly observed in low-dimensional selenoborates (constituting more than half of the 0D selenoborates). All 1D structures have $[BSe_4]$ as the building unit. $[B_7Se_{13}]$ units and supertetrahedral $[B_{10}Se_{20}]$ make up most high-dimensional selenoborates. It is worth noting that, unlike thioborates, selenoborates tend to form high-dimensional structures such as chains and layers, which may be related to the fact that $[BSe_4]$ appears more commonly than $[BSe_3]$ in selenoborates. Specifically, only 3 out of 21 known selenoborates are composed of $[BSe_3]$.

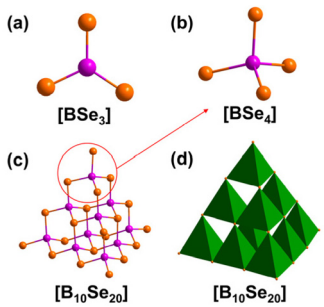

Fig. 3 The structures of (a) $[BSe_3]$, (b) $[BSe_4]$, and (c) and (d) $[B_{10}Se_{20}]$.

3.1. Selenoborates with zero-dimensional structures

To the best of our knowledge, the four 0D selenoborates predominantly feature two types of structural units: $[BSe_3]$ and $[B_{10}Se_{20}]$. Notably, the supertetrahedron $[B_{10}Se_{20}]$ is constructed from corner-sharing $[BSe_4]$ tetrahedra (Fig. 3c and d).

Among these compounds, three exhibit isolated $[BSe_3]$ units with varying dihedral angles: 0° for Tl_3BSe_3, 89.5° for $Ba_7(BSe_3)_4Se$ and 90° for $Ba_3(BSe_3)(SbSe_3)$. The other one is composed of the $[B_{10}Se_{20}]$ supertetrahedron. In these selenoborate structures, the B–Se bond lengths range from 1.91(2) to 2.06 (2) Å.

3.1.1. Selenoborates with mononuclear $[BSe_3]$ clusters. Tl_3BSe_3 [70] crystallizes in the monoclinic space group $P2_1/m$ and represents the first reported selenoborate containing only isolated $[BSe_3]$ as the anion units. The isolated $[BSe_3]$ units are arranged parallel to each other, and are interconnected *via* Tl^+ cations to form the overall framework. In the structure, the B–Se bond lengths are 1.94(2) Å and 1.97(4) Å. The slight elongation of the bond lengths in $[BSe_3]$ may be caused by the relatively high charge on this anion. The Se–B–Se bond angles range from 119(2)° to 121(2)°.

$Ba_7(BSe_3)_4Se$ [71] crystallizes in the monoclinic space group $C2/c$, which is the first reported barium selenoborate. The dihedral angle between planar $[BSe_3]$ units is 89.5°, and isolated $[BSe_3]$ units are interconnected *via* Ba^{2+} cations to form the entire structure (Fig. 4). In the structure, the B–Se bond lengths are 1.938(10) Å and 1.992(10) Å, and the Se–B–Se bond angles range from 115.2(5)° to 123.4(5)°.

3.1.2. The selenoborate with multinuclear $[B_{10}Se_{20}]$ clusters. $Li_{6-2x}Sr_{2+x}B_{10}Se_{20}$ ($x \approx 0.7$) [72] crystallizes in the tetragonal space group $I4_1/a$, which is the first reported selenoborate containing isolated supertetrahedral $[B_{10}Se_{20}]$. In its structure, there are isolated $[B_{10}Se_{20}]$ structures that are formed from tetrahedral $[BSe_4]$ units, and these $[B_{10}Se_{20}]$ units are connected by Li^+ and Sr^{2+} cations to form the entire structure. The average B–Se bond length is 2.055 Å.

3.1.3. The selenoborate with heteronuclear 0D clusters. $Ba_3(BSe_3)(SbSe_3)$ [73] crystallizes in the hexagonal space group

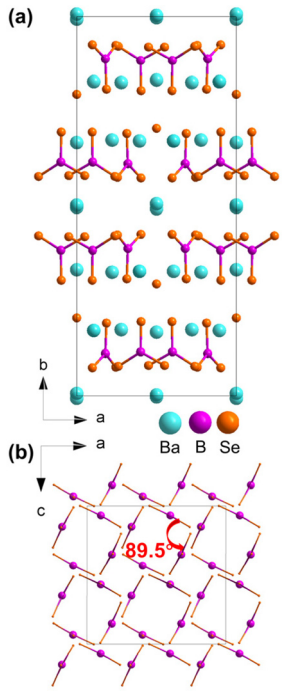

Fig. 4 (a) The whole structure of $Ba_7(BSe_3)_4Se$ and (b) arrangement and dihedral angle between planar $[BSe_3]$ units in $Ba_7(BSe_3)_4Se$.

$P\bar{6}2m$, which is the only example containing heteronuclear 0D clusters. In the structure, there are $[SbSe_3]$ pyramids and isolated $[BSe_3]$ units, and they are connected by Ba^{2+} cations (Fig. 5). The B–Se bond lengths range from 1.91(2) to 2.06(2) Å and the Sb–Se bond lengths range from 2.185(2) to 2.581(2). The Se–B–Se bond angles range from 115.2(9)° to 125.8(8)° and the Se–Sb–Se bond angles range from 91.0(4)° to 176.1(5)°.

3.2. One-dimensional selenoborates

All 1D selenoborates are constructed from the mononuclear cluster $[BSe_4]$ and Se–Se bonds. Specifically, $[BSe_4]$ and Se–Se bonds could form five-membered rings B_2Se_3 and six-membered rings B_2Se_4. These units can be further constructed into polymeric chains $[BSe_3^{3-}]_n$, $[B_2Se_7^{2-}]_n$ and $[B_3Se_{10}^{3-}]_n$ (Fig. 6). The B–Se bond lengths in 1D selenoborates range from 2.017 (17) to 2.358(3) Å. The Se–B–Se bond angles range from 90.5 (4)° to 118.2(4)°.

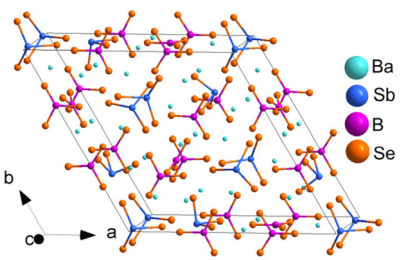

Fig. 5 The structure of $Ba_3(BSe_3)(SbSe_3)$.

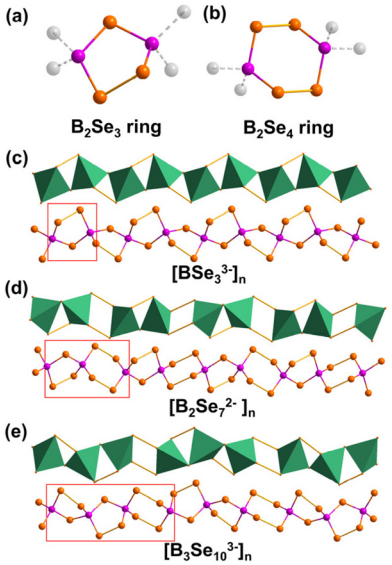

Fig. 6 The structures of (a) the B_2Se_3 five-membered ring, (b) the B_2Se_4 six-membered ring, (c) polymeric chain $[BSe_3^{3-}]_n$, (d) polymeric chain $[B_2Se_7^{2-}]_n$, and (e) polymeric chain $[B_3Se_{10}^{3-}]_n$.

3.2.1. Selenoborates with polymeric $[BSe_3^{3-}]_n$ chains. $CsBSe_3$ and $RbBSe_3$ crystallize in the monoclinic space group $P2_1/c$, and $TlBSe_3$ crystallizes in the monoclinic space group Cc.[74] Besides, they are the first reported selenoborates containing polymeric anionic $[BSe_3^{3-}]_n$ chains. In detail, the $[BSe_4]$ units are connected both through Se–Se bonds and by sharing one vertex Se atom. First, two adjacent $[BSe_4]$ units form a B_2Se_3 five-membered ring, and then B_2Se_3 five-membered rings helically connect and extend to become the polymeric $[BSe_3^{3-}]_n$ chains. In their structures, the Cs^+, Rb^+ and Tl^+ cations are inserted in the spaces between the $[BSe_3^{3-}]_n$ chains in $CsBSe_3$, $RbBSe_3$ and $TlBSe_3$. The B–Se bond lengths in them range from 2.034(17) to 2.358(3) Å and the Se–B–Se bond angles range from 90.5(4)° to 113.4(4)°.

3.2.2. Selenoborates with polymeric $[B_2Se_7^{2-}]_n$ chains. $Na_2B_2Se_7$, $K_2B_2Se_7$,[75] $Rb_2B_2Se_7$ and $Tl_2B_2Se_7$ [76] all crystallize in the monoclinic space group $C2/c$. In their structures, the B_2Se_3 five-membered rings and six-membered rings connect alternately with a ratio of 1 : 1 to form $[B_2Se_7^{2-}]_n$ chains, and the Na^+, K^+, Rb^+ and Tl^+ cations are situated between the polymeric $[B_2Se_7^{2-}]_n$ chains. The B–Se bond lengths in this series of structures range from 2.021(8) to 2.062(14) Å. The Se–B–Se bond angles range from 94.3(4)° to118.2(4)°. The Se–Se bond lengths in them range from 2.3630(14) to 2.3690(19) Å.

3.2.3. Selenoborates with polymeric $[B_3Se_{10}^{3-}]_n$ chains. $Cs_3B_3Se_{10}$ and $Tl_3B_3Se_{10}$ [76] crystallize in the triclinic space group $P\bar{1}$, and they are the first reported selenoborates containing polymeric $[B_3Se_{10}^{3-}]_n$ anionic chains. Therein, the B_2Se_3 five-membered rings and six-membered rings occur in a ratio of 2 : 1, and two five-membered rings and one six-membered ring act as the repeatable section in the infinite $[B_3Se_{10}^{3-}]_n$ chain. The Cs^+ and Tl^+ cations are located between the poly-

meric chains to balance the charge and hold the structure together. The B–Se bond lengths in them range from 2.017(17) to 2.097(17) Å. The Se–B–Se bond angles range from 94.4(5)° to 116.2(8)°. The Se–Se bond lengths in them range from 2.3396 (14) to 2.380(2) Å.

3.3. Two-dimensional selenoborates

The 2D selenoborates are composed of only two types of building units: tetrahedral [BSe_4] and supertetrahedral [$B_{10}Se_{20}$]. In these 2D selenoborates, the B–Se bond lengths range from 2.032(7) to 2.080(7) Å. The Se–B–Se bond angles range from 94.4(5)° to 116.2(8)°.

3.3.1. Selenoborates with 2D polymers constructed from tetrahedral [BSe_4]. $Ba_2B_4Se_{13}$ [77] crystallizes in the monoclinic space group $P2_1/c$, which is the first reported alkaline earth perselenoborate. In the structure of $Ba_2B_4Se_{13}$, there are B_2Se_3 five-membered and B_2Se_4 six-membered rings composed of [BSe_4] units and Se–Se bonds. Specifically, a segment of the B_2Se_3 five-membered ring formally opens up, establishing diselenide bridges to neighboring chains. Consequently, 2D polymeric $[(B_4Se_{13})^{4-}]_n$ layers are formed (Fig. 7). The B–Se bond lengths range from 2.032(7) to 2.080(7) Å. The Se–B–Se bond angles range from 94.4(5)° to 116.2(8)°. The Se–Se bond lengths range from 2.370(1) to 2.380(1) Å.

BaB_2Se_6 [77] crystallizes in the orthorhombic space group *Cmca* and is the first reported selenoborate containing the B_2Se_2 four-membered rings. In the structure of BaB_2Se_6, four-membered B_2Se_2 rings and B_6Se_{10} macrocycles form voids, and Ba^{2+} cations are located in the voids (Fig. 8). The B–Se bond lengths range from 2.038(3) to 2.073(4) Å. The Se–B–Se bond angles range from 101.4(3)° to 115.4(3)°. The Se–Se bond length is 2.361(1) Å. Specifically, the bond angle (76.7(3)°) within the B_2Se_2 four-membered rings is much smaller than that in the B_2Se_3 five-membered rings (94° in $[B_2Se_7^{2-}]_n$), and the B–Se bond length within the B_2Se_2 four-membered rings (2.073(4) Å) is longer than that of the diselenide bridges (2.038 (3) Å).

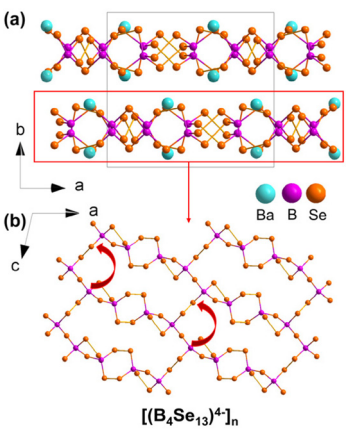

Fig. 7 The structures of (a) the $Ba_2B_4Se_{13}$ layer and (b) the $[(B_4Se_{13})^{4-}]_n$ layer.

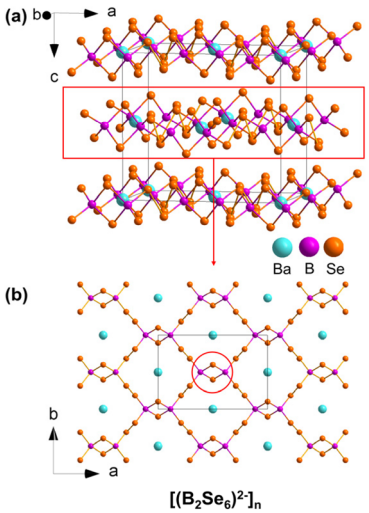

Fig. 8 The structures of (a) the BaB_2Se_6 layer and (b) the $[(B_2Se_6)^{2-}]_n$ layer.

3.3.2. Selenoborates with 2D polymers constructed from supertetrahedral [$B_{10}Se_{20}$]. $Li_{6-x}Cs_xB_{10}Se_{18}$ ($x \approx 1$)[78] crystallizes in the tetragonal space group $I4_1/amd$ and is the only 2D selenoborate containing T3 supertetrahedral [$B_{10}Se_{20}$]. In its structure, the supertatrahedra [$B_{10}Se_{20}$] are corner-sharing to form layers (Fig. 9), between which are located the Li^+ and Cs^+ cations. The B–Se bond lengths range from 2.038(3) to 2.073(4) Å. The Se–B–Se bond angles range from 101.4(3)° to 115.4(3)°.

3.4. Three-dimensional selenoborates

In addition to the most common tetrahedral [BSe_4] and supertetrahedral [$B_{10}Se_{20}$] units, the [B_7Se_{13}] unit represents a distinctive feature among 3D selenoborates, with no analogous configuration found in thioborates. The [B_7Se_{13}] unit is found in the zeolite-like compound $Li_7B_7Se_{15}$. Fig. 10 illustrates the intricate constructional framework of B_4Se_{13} basic units. Originating from a central μ4-selenium atom, these units integrate with four [BSe_4] tetrahedra in the initial shell. The interconnection of the tetrahedra in the second shell is facilitated by two [BSe_4] entities from the first inner shell. Additionally, a bridging [BSe_4] tetrahedron from this second outer shell establishes connectivity among the basic units within the anion network.

3.4.1. Selenoborates with 3D polymeric networks constructed from [BSe_4]. $CuBSe_2$ [79,80] crystallizes in the tetragonal space group $I\bar{4}2d$ and is the only chalcopyrite-type semi-

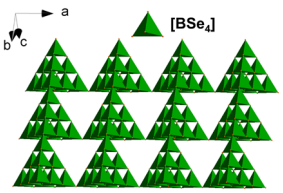

Fig. 9 The layer in the structure of $Li_{6-x}Cs_xB_{10}Se_{18}$ ($x \approx 1$).

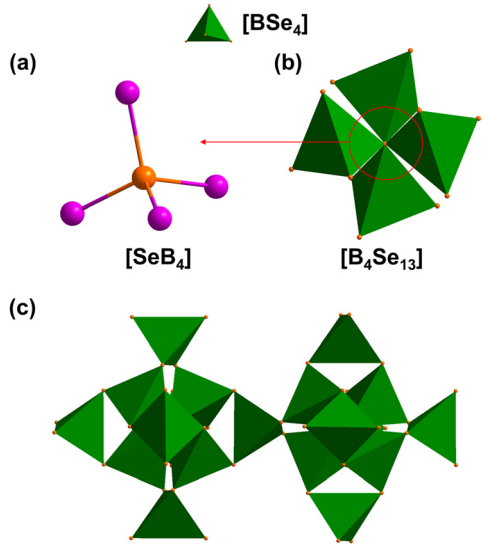

Fig. 10 Basic building block of the $B_7Se_{13}^{5-}$ anion in $Li_7B_7Se_{15}$. (a) SeB_4 tetrahedron forming (b) B_4Se_{13} basic units interconnected *via* additional BSe units to (c) $B_7Se_{13}^{5-}$ entities forming the network.

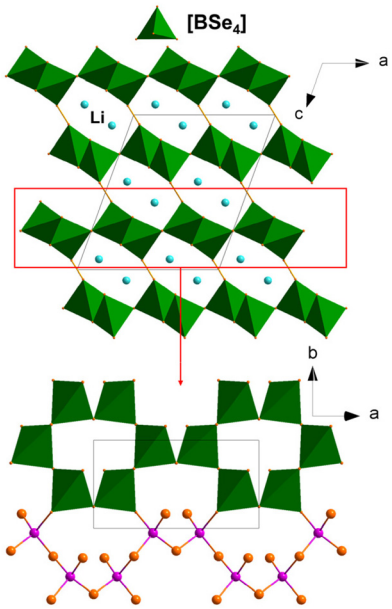

Fig. 11 The structure of $Li_2B_2Se_5$.

conductor among selenoborates. In its structure, there are $[BSe_4]$ units connected by sharing corners to form a 3D network with Cu^{2+} cations distributed throughout. The band gap of nanocrystalline $CuBSe_2$ has been studied, and the experimental band gap is 3.13 eV.

$Li_2B_2Se_5$ [81] crystallizes in the monoclinic space group $C2/c$ and is the first perselenoborate with a 3D anion network. In its structure, one $[BSe_4]$ unit shares three vertex Se atoms with neighboring $[BSe_4]$ units to form polymeric B–Se layers, which exhibit twelve-membered B_6Se_6 rings. These layers are connected by Se–Se bonds to form a 3D network (Fig. 11). The average B–Se bond length is 2.061 Å.

3.4.2. Selenoborates with 3D polymeric networks constructed from $[B_7Se_{13}]$. $Li_7B_7Se_{15}$ [82] crystallizes in the tetragonal space group $P4_2/nbc$ and is a novel zeolite-like selenoborate. The structure of $Li_7B_7Se_{15}$ comprises $([B_7Se_{13}]^{5-})_n$, diselenide Se_2^{2-} and Li^+ cations. Alternatively, it could be described as an intercalation compound "$Li_5B_7Se_{13}$" with additional diselenide "Li_2Se_2". The B–Se bond lengths range from 2.027(2) to 2.150(2) Å. The Se–B–Se bond angles range from 103.7° to 116.0°, which is consistent with the ideal tetrahedral angle (109.6°). The Se–Se bond length in "Li_2Se_2" is 2.3643(5) Å.

3.4.3. Selenoborates with 3D polymeric networks constructed from $[B_{10}Se_{20}]$. $Na_6B_{10}Se_{18}$ [83] crystallizes in the tetragonal space group $I4_1/acd$. In its structure, supertetrahedral $[B_{10}Se_{20}]$ units are connected by sharing corners to form an anionic network and Na^+ cations are located in the large voids between the anionic network to form a 3D network. The anionic network in $Na_6B_{10}Se_{18}$ is composed of infinite polymeric anions of formula $([B_{10}Se_{16}Se_{4/2}]^{6-})_\infty$. The B–Se bond lengths range from 2.020(5) to 2.083(7) Å. The Se–B–Se bond angles range from 100.4(3)° to 114.0(4)°, which is nearly exactly the ideal tetrahedral angle (109.6°). Supertetrahedral $[B_{10}Se_{20}]$ units can be found not only in 0D and 2D selenoborates, but also in selenoborates formed by a 3D polymeric network, which is special compared with the structure features of thioborates and borates.

$Li_{6+2x}[B_{10}Se_{18}]Se_x$ ($x \approx 2$) [84] crystallizes in the monoclinic space group $C2/c$. In its structure, corner-sharing supertetrahedral $[B_{10}Se_{20}]$ units form a 3D anionic network, of which partially occupied Li^+ and additional disordered Se^{2-} are located in the channels. The B–Se bond lengths range from 2.006(9) to 2.077(9) Å. The Se–B–Se bond angles range from 99.4(4)° to 116.3(4)°.

3.5. Selenoborate-*closo*-dodecaborates

Advancements in boron chemistry have led to the discovery of selenoborate-*closo*-dodecaborates as a distinct family within this field. Due to the lack of electrons in its outer shell, boron tends to form a framework that allows it to share electrons efficiently and achieve a more stable structure. The highly symmetrical B_{12} icosahedron is commonly found in many boron compounds because of its exceptional stability. $Cs_8[B_{12}(BSe_3)_6]$ [85] and $Rb_8[B_{12}(BSe_3)_6]$ [86] crystallize in the triclinic space group $P\bar{1}$, representing the first reported selenoborate-*closo*-dodecaborates (Fig. 12). In their structures, the icosahedral B_{12} cluster is completely saturated with $[BSe_3]$ units, resulting in a novel configuration within the selenoborate system.

$Rb_4Hg_2[B_{12}(BSe_3)_6]$ and $Cs_4Hg_2[B_{12}(BSe_3)_6]$ [86] crystallize in the triclinic space group $P\bar{1}$ and are the first transition metal selenoborates. In their structures, there is no direct linkage between isolated anion moieties. The B–Se bond lengths in them range from 1.915(11) to 2.006(8) Å. The B–B bond lengths in them range from 1.750(13) to 1.809(19) Å.

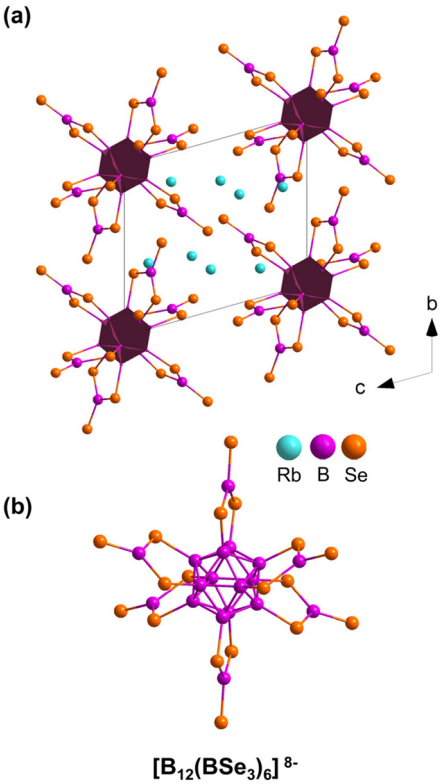

Fig. 12 The structures of (a) the $Rb_8[B_{12}(BSe_3)_6]$ and (b) the $[B_{12}(BSe_3)_6]^{8-}$ unit.

$Na_6[B_{18}Se_{17}]$ [87] crystallizes in the monoclinic space group *C*2/*c* and is the first boron selenium compound with a polymeric anionic cluster chain $([B_{18}Se_{16}Se_{2/2}]^{6-})_\infty$.

$K_8[B_{12}(BSe_3)_6]$ [88] crystallizes in the monoclinic space group *Cm* and is the first selenoborate-*closo*-dodecaborate with three different anion substitution patterns. $Na_8[B_{12}(BSe_3)_6]$ [89] crystallizes in the monoclinic space group $P2_1/c$. There are isolated $[B_{12}(BSe_3)_6]$ and Na^+ cations in its structure.

$Na_2[B_{18}Se_{16}]$ [90] crystallizes in the trigonal space group $P\bar{3}$. Formed by icosahedral B_{12} clusters and saturated $[BSe_3]$ units, the cluster entities $[B_{12}(BSe_3)_6]$ are connected to each other through Se–Se bonds, thus forming a 3D network with $[(B_{18}Se_{12}Se_{6/2})_n]^{2-}$ and $[(B_{18}Se_{15}Se_{6/2})_n]^{2-}$ anions in a ratio of 2 : 1.

4. Properties

For IR functional materials, the bandgap is one of the key performance indicators. Research on the properties of selenoborates remains relatively scarce, and only the bandgap of $CuBSe_2$ has been estimated at 3.13 eV from its diffuse reflectance spectrum. To further explore the optical properties of the reported selenoborates, we calculated the bandgaps of selected alkali/alkaline earth metal selenoborates with ordered structures using the generalized gradient approximation (GGA) and the Heyd–Scuseria–Ernzerhof (HSE06) hybrid functional (Table 2).

Table 2 The calculated bandgaps of selected selenoborates

Formula	Building unit	E_g (GGA)	E_g (HSE06)
$Na_2B_2Se_7$[a]	$[BSe_4]$	1.67 eV	2.49 eV
$K_2B_2Se_7$[a]	$[BSe_4]$	1.84 eV	2.73 eV
$Ba_7(BSe_3)_4Se$	$[BSe_3]$	2.20 eV	2.91 eV
$CsBSe_3$[a]	$[BSe_4]$	1.84 eV	2.66 eV
$RbBSe_3$[a]	$[BSe_4]$	1.68 eV	2.50 eV
$Li_2B_2Se_5$[a]	$[BSe_4]$	1.72 eV	2.56 eV
$Cs_3B_3Se_{10}$[a]	$[BSe_4]$	1.89 eV	2.75 eV
$Rb_2B_2Se_7$[a]	$[BSe_4]$	1.93 eV	2.83 eV
BaB_2Se_6[a]	$[BSe_4]$	1.78 eV	2.63 eV
$Ba_2B_4Se_{13}$[a]	$[BSe_4]$	1.42 eV	2.18 eV

[a] The compounds with Se–Se bonds in the structures.

The majority of selected selenoborates exhibit HSE06 bandgaps exceeding 2.5 eV, thereby meeting the requirements for IR functional materials. Notably, the bandgap of the compound $Ba_7(BSe_3)_4Se$, which contains $[BSe_3]$ as functional units, is larger than that of other compounds containing $[BSe_4]$ units. Furthermore, among isomorphic selenoborates containing Se–Se bonds, those with heavier cations display larger bandgaps. This anomalous behavior may be attributed to the interaction between cations and Se–Se bonds.

In order to evaluate their potential as IR NLO materials, we calculated the SHG coefficients of $CuBSe_2$ ($I\bar{4}2m$, NCS) and $TlBSe_3$ (*Cc*, NCS). Specifically, the results show that $CuBSe_2$ (d_{33} = −11.17 pm V^{-1}) and $TlBSe_3$ (d_{13} = 35.39 pm V^{-1}) exhibit SHG properties of about 0.8 × AGS and 2.6 × AGS, respectively. This indicates the potential of selenoborates as IR NLO materials. Furthermore, their SHG properties may originate from the good arrangement of $[BSe_3]$ units in their structures.

5. Summary and perspectives

In summary, this paper presents a comprehensive overview of the structures of reported selenoborates, along with their synthesis methods. The selenoborates are primarily based on two fundamental structural units: $[BSe_3]$ and $[BSe_4]$, which, along with Se–Se bonds, form a variety of structural frameworks, including $[B_{10}Se_{20}]$ supertetrahedra, $[BSe_3^{3-}]_n$, $[B_2Se_7^{2-}]_n$ and $[B_3Se_{10}^{3-}]_n$ polymeric chains, $[(B_4Se_{13})^{4-}]_n$ and $[(B_2Se_6)^{2-}]_n$ layers and so on. Compared to borates and thioborates, selenoborates exhibit considerable potential for structural diversity, which remains largely unexplored and is worthy of further investigation.

Most selenoborates are synthesized *via* solid-state reactions involving metal selenides, amorphous boron, and selenium in evacuated carbon-coated silica tubes, typically at temperatures of 600–950 °C. Obtaining highly pure selenoborates with well-defined structures is challenging due to the reactivity of boron chalcogenides with container materials at elevated temperatures.

What is more, the analysis of microstructural performances of related units has shown that the $[BSe_3]$ unit exhibits the

highest polarizability anisotropy and hyperpolarizability, highlighting its potential as a good seed for IR functional materials. The DFT calculations illustrated that selected alkali/alkaline earth metal selenoborates have large bandgaps and could meet the requirements for IR functional materials. Notably, reported NCS selenoborates exhibit significant SHG coefficients, highlighting the potential of selenoborates as IR NLO materials. Furthermore, selenoborates containing the $[BSe_3]$ unit may exhibit larger bandgaps. With targeted efforts in the following areas, further enhancements are anticipated.

(i) Current research on the properties of selenoborates is relatively sparse, highlighting the need for further investigation into their structure–property relationships. Notably, the common presence of Se–Se bonds within the selenoborate system has been discovered. While the effects of the Se–Se bonds on structures and properties remain not fully elucidated, these are worth exploring in the future.

(ii) The π-conjugated $[BSe_3]$ unit shows good microstructural performance with large polarizability anisotropy and hyperpolarizability. Considering thioborates such as $NaBaBS_3$, $LaBS_3$, $NaSrBS_3$ and so on that comprise planar triangular $[BS_3]$ as building units exhibit good properties, the exploration of more selenoborates containing $[BSe_3]$ units may help in the discovery of high-performance functional materials.

(iii) Structural analysis of selenoborates shows that none of the reported selenoborates are composed of mixed anionic groups $[BSe_3]$ and $[BSe_4]$. It is known that thioborates composed of mixed anionic groups $[BS_3]$ and $[BS_4]$ all crystallize in NCS space groups. Therefore, synthesizing selenoborates with both $[BSe_3]$ and $[BSe_4]$ building units opens up vast possibilities for exploring novel NCS structures and enhancing the NLO properties of selenoborates.

(iv) The currently reported synthesis methods for selenoborates mainly use metal selenides as raw materials, which means high costs when growing crystals. The improvement of synthesis methods will bring new opportunities for the application of selenoborates.

(v) Among the 21 reported selenoborates, most are ternary compounds, predominantly featuring cations that are alkali or alkaline earth metals. In these structures, the arrangement of anions is primarily regulated by the presence of a single type of cation. Derived from this, the exploration of quaternary and multi-selenoborates warrants investigation. The incorporation of more diverse cations may provide more possibilities for regulating the structure, thereby enhancing the structural diversity of the selenoborate system.

Data availability

All the data were extracted from cited articles.

Conflicts of interest

There are no conflicts to declare.

Acknowledgements

This work was supported by the National Natural Science Foundation of China (22305264, 22335007, 61835014), the Xinjiang Major Science and Technology Project (2021A01001), the Natural Science Foundation of the Xinjiang Uygur Autonomous Region (2022D01A333), the Key Laboratory Opening Foundation of the Xinjiang Uygur Autonomous Region (2022D04013), and the China Postdoctoral Science Foundation (2023T100679).

References

1 A. L. Schawlow and C. H. Townes, Infrared and Optical Masers, *Phys. Rev.*, 1958, **112**, 1940–1949.
2 T. H. Maiman, Stimulated Optical Radiation in Ruby, *Nature*, 1960, **187**, 493–494.
3 P. A. Franken, A. E. Hill, C. W. Peters and G. Weinreich, Generation of Optical Harmonics, *Phys. Rev. Lett.*, 1961, **7**, 118–119.
4 V. G. Dmitriev, G. G. Gurzadyan and D. N. Nikogosyan, *Handbook of nonlinear optical crystals*, Springer, Berlin, 2013.
5 D. N. Nikogosyan, *Nonlinear optical crystals: a complete survey*, Springer Science & Business Media, 2006.
6 L. E. Myers, R. C. Eckardt, M. M. Fejer, R. L. Byer, W. R. Bosenberg and J. W. Pierce, Quasi-phase-matched optical parametric oscillators in bulk periodically poled $LiNbO_3$, *J. Opt. Soc. Am. B*, 1995, **12**, 2102–2116.
7 H. Yuan, P. Huang, T. Feng, Y. Ma, X. Wang, H. Cao, Y. Wang, W. Zhao and Y. Fu, Efficient single-cycle mid-infrared femtosecond laser pulse generation by spectrally temporally cascaded optical parametric amplification with pump energy recycling, *Opt. Lett.*, 2024, **49**, 2269–2272.
8 X. Wang, X. Leng, Y. Kuk, J. Lee, Q. Jing and K. M. Ok, Deep-Ultraviolet Transparent Mixed Metal Sulfamates with Enhanced Nonlinear Optical Properties and Birefringence, *Angew. Chem., Int. Ed.*, 2024, **63**, e202315434.
9 T. Wu, X. Jiang, K. Duanmu, C. Wu, Z. Lin, Z. Huang, M. G. Humphrey and C. Zhang, Secondary-Bond-Driven Construction of a Polar Material Exhibiting Strong Broad-Spectrum Second-Harmonic Generation and Large Birefringence, *Angew. Chem., Int. Ed.*, 2024, **63**, e202318107.
10 X. Zhao, C. Lin, C. Wang, H. Tian, T. Yan, B. Li, N. Ye and M. Luo, Molecular Crystals Constructed by Polar Molecular Cages: A Promising System for Exploring High-performance Infrared Nonlinear Optical Crystals, *Angew. Chem., Int. Ed.*, 2024, **63**, e202319424.
11 H. Wu, S. Pan, K. R. Poeppelmeier, H. Li, D. Jia, Z. Chen, X. Fan, Y. Yang, J. M. Rondinelli and H. Luo, $K_3B_6O_{10}Cl$: A New Structure Analogous to Perovskite with a Large Second Harmonic Generation Response and Deep UV Absorption Edge, *J. Am. Chem. Soc.*, 2011, **133**, 7786–7790.
12 H. Wu, H. Yu, Z. Yang, X. Hou, X. Su, S. Pan, K. R. Poeppelmeier and J. M. Rondinelli, Designing a Deep-

Ultraviolet Nonlinear Optical Material with a Large Second Harmonic Generation Response, *J. Am. Chem. Soc.*, 2013, **135**, 4215–4218.

13 G. Zou, N. Ye, L. Huang and X. Lin, Alkaline-Alkaline Earth Fluoride Carbonate Crystals $ABCO_3F$ (A = K, Rb, Cs; B = Ca, Sr, Ba) as Nonlinear Optical Materials, *J. Am. Chem. Soc.*, 2011, **133**, 20001–20007.

14 G. Zou and K. M. Ok, Novel ultraviolet (UV) nonlinear optical (NLO) materials discovered by chemical substitution-oriented design, *Chem. Commun.*, 2020, **11**, 5404–5409.

15 H. Liu, Q. Wu, L. Liu, Z. Lin, P. S. Halasyamani, X. Chen and J. Qin, $AgBi(SO_4)(IO_3)_2$: aliovalent substitution induces structure dimensional upgrade and second harmonic generation enhancement, *Chem. Commun.*, 2021, **57**, 3712–3715.

16 H. Liu, X. Jiang, X. Wang, L. Yang, Z. Lin, Z. Hu, X. Meng, X. Chen and J. Qin, Influence of A-site cations on germanium iodates as mid-IR nonlinear optical materials: $A_2Ge(IO_3)_6$ (A = Li, K, Rb and Cs) and $BaGe(IO_3)_6{\cdot}H_2O$, *J. Mater. Chem. C*, 2018, **6**, 4698–4705.

17 Y. Chen, C. Hu, Z. Fang and J. Mao, $K_2Pb(H_2C_3N_3O_3)_4(H_2O)_4$: a potential UV nonlinear optical material with large birefringence, *Inorg. Chem. Front.*, 2021, **8**, 3547–3555.

18 B. Wu, C. Hu, R. Tang, F. Mao, J. Feng and J. Mao, Fluoroborophosphates: a family of potential deep ultraviolet NLO materials, *Inorg. Chem. Front.*, 2019, **6**, 723–730.

19 Y. Hu, X. Xu, R. Wang, J. Han, S. Zhang, S. Zhan, J. Guo, L. M. Wu and L. Chen, $[Sn_3OF]PO_4$ vs. $[Sn_3F_3]PO_4$: enhancing birefringence by breaking the R3 symmetry and realigning lone pairs, *Inorg. Chem. Front.*, 2024, **11**, 5648–5656.

20 Z. Yu, Q. Ding, Y. Jiang, W. Huang, C. Yang, S. Zhao and J. Luo, $Na_{10}Zn(NO_3)_4(SO_3S)_4$: a nonlinear optical crystal combining inorganic π-conjugated and non-π-conjugated heteroanion groups, *Inorg. Chem. Front.*, 2024, **11**, 107–113.

21 X. Du, F. Wang, F. Liang, Z. Hu, Y. Wu and X. Zhang, $A_{0.5}H_2C_6N_7O_3{\cdot}4H_2O$ (A = Ca^{2+}, Sr^{2+}) iso-cyamelurates with ultra-large π-conjugated group and excellent nonlinear optical properties, *Inorg. Chem. Front.*, 2023, **10**, 5979–5985.

22 S. Yu, J. Fan, Z. Hu and Y. Wu, $Li_3Na_7B_4P_6O_{26}$: a new ultraviolet transparent congruently melting non-linear optical crystal, *Dalton Trans.*, 2024, **53**, 12331–12337.

23 P. Feng, J.-X. Zhang, M.-Y. Ran, X.-T. Wu, H. Lin and Q.-L. Zhu, Rare-earth-based chalcogenides and their derivatives: an encouraging IR nonlinear optical material candidate, *Chem. Commun.*, 2024, **15**, 5869–5896.

24 G. Li, Z. Yang, J. Li and S. Pan, A review of the AB(II)C(IV)D family as infrared nonlinear optical materials: the effect of each site on the structure and optical properties, *Chem. Commun.*, 2020, **56**, 11565–11576.

25 M. Mutailipu, K. R. Poeppelmeier and S. Pan, Borates: A Rich Source for Optical Materials, *Chem. Rev.*, 2021, **121**, 1130–1202.

26 P.-F. Liu, Y.-Y. Li, Y.-J. Zheng, J.-S. Yu, R.-H. Duan, H. Chen, H. Lin, L. Chen and L.-M. Wu, Tailored synthesis of nonlinear optical quaternary chalcohalides: $Ba_4Ge_3S_9Cl_2$, $Ba_4Si_3Se_9Cl_2$ and $Ba_4Ge_3Se_9Cl_2$, *Dalton Trans.*, 2017, **46**, 2715–2721.

27 K. Feng, L. Kang, Z. Lin, J. Yao and Y. Wu, Noncentrosymmetric chalcohalide $NaBa_4Ge_3S_{10}Cl$ with large band gap and IR NLO response, *J. Mater. Chem. C*, 2014, **2**, 4590–4596.

28 B. Zhang, G. Shi, Z. Yang, F. Zhang and S. Pan, Fluorooxoborates: Beryllium-Free Deep-Ultraviolet Nonlinear Optical Materials without Layered Growth, *Angew. Chem., Int. Ed.*, 2017, **56**, 3916–3919.

29 G. Shi, Y. Wang, F. Zhang, B. Zhang, Z. Yang, X. Hou, S. Pan and K. R. Poeppelmeier, Finding the Next Deep-Ultraviolet Nonlinear Optical Material: $NH_4B_4O_6F$, *J. Am. Chem. Soc.*, 2017, **139**, 10645–10648.

30 X. Wang, Y. Wang, B. Zhang, F. Zhang, Z. Yang and S. Pan, CsB_4O_6F: A Congruent-Melting Deep-Ultraviolet Nonlinear Optical Material by Combining Superior Functional Units, *Angew. Chem., Int. Ed.*, 2017, **56**, 14119–14123.

31 M. Mutailipu, M. Zhang, B. Zhang, L. Wang, Z. Yang, X. Zhou and S. Pan, $SrB_5O_7F_3$ Functionalized with $[B_5O_9F_3]^{6-}$ Chromophores: Accelerating the Rational Design of Deep-Ultraviolet Nonlinear Optical Materials, *Angew. Chem., Int. Ed.*, 2018, **57**, 6095–6099.

32 Y. Wang, B. Zhang, Z. Yang and S. Pan, Cation-Tuned Synthesis of Fluorooxoborates: Towards Optimal Deep-Ultraviolet Nonlinear Optical Materials, *Angew. Chem., Int. Ed.*, 2018, **57**, 2150–2154.

33 X. Chen, B. Zhang, F. Zhang, Y. Wang, M. Zhang, Z. Yang, K. R. Poeppelmeier and S. Pan, Designing an Excellent Deep-Ultraviolet Birefringent Material for Light Polarization, *J. Am. Chem. Soc.*, 2018, **140**, 16311–16319.

34 Z. Zhang, Y. Wang, B. Zhang, Z. Yang and S. Pan, Polar Fluorooxoborate, NaB_4O_6F: A Promising Material for Ionic Conduction and Nonlinear Optics, *Angew. Chem., Int. Ed.*, 2018, **57**, 6577–6581.

35 G. Sun, X. Qi, H. Wu, Z. Hu, J. Wang and Y. Wu, New ultraviolet transparent rare-earth borates with enhanced birefringence induced by cation chemical substitution, *Inorg. Chem. Front.*, 2024, **11**, 3245–3253.

36 J. Guo, A. Tudi, S. Han, Z. Yang and S. Pan, $Sn_2B_5O_9Cl$: A Material with Large Birefringence Enhancement Activated Prepared via Alkaline-Earth-Metal Substitution by Tin, *Angew. Chem., Int. Ed.*, 2019, **58**, 17675–17678.

37 F. Liang, L. Kang, Z. Lin and Y. Wu, Mid-Infrared Nonlinear Optical Materials Based on Metal Chalcogenides: Structure–Property Relationship, *Cryst. Growth Des.*, 2017, **17**, 2254–2289.

38 N. Zhao, D. Lu, J. Xu, K. Wu, H. Yu and H. Zhang, Greatly enhanced optical anisotropy in thiophosphates inspired by rational coupling of tetrahedra and ethane-like $[P_2S_6]^{4-}$ groups, *Inorg. Chem. Front.*, 2024, **11**, 4603–4610.

39 J. Xu, K. Wu, B. Zhang, H. Yu and H. Zhang, $LaAeAl_3S_7$ (Ae = Ca, Sr): Cairo pentagonal layered thioaluminates achieving a good balance between a strong second harmonic generation response and a wide bandgap, *Inorg. Chem. Front.*, 2023, **10**, 2045–2052.

40 K. Feng, X. Jiang, L. Kang, W. Yin, W. Hao, Z. Lin, J. Yao, Y. Wu and C. Chen, Ba6Sn6Se13: a new mixed valence selenostannate with NLO property, *Dalton Trans.*, 2013, **42**, 13635–13641.

41 J. R. Glenn, J. B. Cho, Y. Wang, A. J. Craig, J.-H. Zhang, M. Cribbs, S. S. Stoyko, K. E. Rosello, C. Barton, A. Bonnoni, P. Grima-Gallardo, J. H. MacNeil, J. M. Rondinelli, J. I. Jang and J. A. Aitken, $Cu_4MnGe_2S_7$ and Cu_2MnGeS_4: two polar thiogermanates exhibiting second harmonic generation in the infrared and structures derived from hexagonal diamond, *Dalton Trans.*, 2021, **50**, 17524–17537.

42 L. S. Breton, G. Morrison, M. R. Lacroix, P. S. Halasyamani and H. C. zur Loye, Lanthanide thioborates, an emerging class of nonlinear optical materials, efficiently synthesized using the boron–chalcogen mixture method, *Chem. Commun.*, 2022, **58**, 7992–7995.

43 Y.-X. Han, C.-L. Hu, Z. Fang, Q.-Q. Chen, B.-X. Li, Y. Lin and J.-G. Mao, $LaBS_3$ revisited: a promising mid-infrared nonlinear optical material, *J. Mater. Chem. C*, 2022, **10**, 12556–12559.

44 J. Zhou, X. Su, L. Luo, J. Li and F. Yu, $MB_3P_2S_{10}$ (M = Rb, Cs): two new alkali metal thioboratephosphates with $[B_6P_4S_{20}]$ T_3-supertetrahedra, *Dalton Trans.*, 2023, **52**, 11401–11406.

45 J. Zhou, K. Hou, Y. Chu, Z. Yang, J. Li and S. Pan, $AIB_3IIC_2IIIQ_6VIXVII$: A Thioborate Halide Family for Developing Wide Bandgap Infrared Nonlinear Materials by Coupling Planar $[BS_3]$ and Polycations, *Small*, 2024, **20**, 2308806.

46 Y. K. Lian, L. M. Wu and L. Chen, Thioborates: potential nonlinear optical materials with rich structural chemistry, *Dalton Trans.*, 2017, **46**, 4134–4147.

47 J. Zhou, L. Wang, H. Wang, L. Luo, J. Li and F. Yu, $Ba_3(BS_3)(PS_4)$: the first alkaline-earth metal thioborate–thiophosphate with strong optical anisotropy originating from planar $[BS_3]$ units, *Dalton Trans.*, 2023, **52**, 16113–16117.

48 Y. Kim, S. W. Martin, K. M. Ok and P. S. Halasyamani, Synthesis of the Thioborate Crystal $ZnxBa_2B_2S_{5+x}$ ($x \approx 0.2$) for Second Order Nonlinear Optical Applications, *Chem. Mater.*, 2005, **17**, 2046–2051.

49 G. Li, J. Li, K. Wu, Z. Yang and S. Pan, $Ba_4(BS_3S)_2S_4$: a new thioborate with unprecedented $[BS_3$-S] and $[S_4]$ fundamental building blocks, *Chem. Commun.*, 2019, **55**, 14793–14796.

50 Y. Yun, M. Wu, C. Xie, Z. Yang, G. Li and S. Pan, Theoretical Prediction-Assisted Synthesis and Characterization of Infrared Nonlinear Optical Material $NaSrBS_3$, *Adv. Opt. Mater.*, 2023, **11**, 2300256.

51 Y. Huang, Y. Zhang, D. Chu, Z. Yang, G. Li and S. Pan, HgB_2S_4: A d_{10} Metal Thioborate with Giant Birefringence and Wide Band Gap, *Chem. Mater.*, 2023, **35**, 4556–4563.

52 Y.-X. Han, C.-L. Hu and J.-G. Mao, $Ca_2Ln(BS_3)(SiS_4)$ (Ln = La, Ce, and Gd): Mixed Metal Thioborate-Thiosilicates as Well-Performed Infrared Nonlinear Optical Materials, *Small*, 2024, **20**, 2305828.

53 Y. Yun, X. Hou, Z. Yang, G. Li and S. Pan, $[RbSr_3X][(BS_3)_2]$ (X = Cl, Br): two salt-inclusion thioborates with large birefringence and structure transformation from centrosymmetric to asymmetric, *Chem. Commun.*, 2024, **60**, 118–121.

54 Y. Yun, W. Xie, Y. Huang, Z. Yang, K. Wu, G. Li and S. Pan, $NaBaBS_3$: A Promising Infrared Functional Material with Large Birefringence Induced by π-Conjugated $[BS_3]$ Units, *Chem. Mater.*, 2022, **34**, 5215–5223.

55 J. Zhou, Y. Chu, J. Li and S. Pan, Ba_2BS_3Cl and $Ba_5B_2S_8Cl_2$: first alkaline-earth metal thioborate halides with $[BS_3]$ units, *Chem. Commun.*, 2021, **57**, 6440–6443.

56 B. M. Oxley, K.-H. Lee, T. S. Ie, J. M. Lee, M. J. Waters, J. M. Rondinelli, J. I. Jang and M. G. Kanatzidis, Structure, Second-, and Third-Harmonic Generation of $Li_4P_2S_6$: A Wide Gap Material with a High Laser-Induced Damage Threshold, *Chem. Mater.*, 2023, **35**, 7322–7332.

57 I. Chung and M. G. Kanatzidis, Metal Chalcogenides: A Rich Source of Nonlinear Optical Materials, *Chem. Mater.*, 2013, **26**, 849–869.

58 B.-W. Liu, H.-Y. Zeng, X.-M. Jiang, G.-E. Wang, S.-F. Li, L. Xu and G.-C. Guo, $[A_3X][Ga_3PS_8]$ (A = K, Rb; X = Cl, Br): promising IR non-linear optical materials exhibiting concurrently strong second-harmonic generation and high laser induced damage thresholds, *Chem. Commun.*, 2016, **7**, 6273–6277.

59 J. Zhou, Z. Fan, K. Zhang, Z. Yang, S. Pan and J. Li, $Rb_2CdSi_4S_{10}$: novel $[Si_4S_{10}]$ T_2-supertetrahedra-contained infrared nonlinear optical material with large band gap, *Mater. Horiz.*, 2023, **10**, 619–624.

60 K. Wu, B. Zhang, Z. Yang and S. Pan, Remarkable multimember-ring configurations in a new family of $Na_7MIISb_5S_{12}$ (MII = Zn, Cd, Hg) exhibiting various three-dimensional tunnel structures, *Chem. Commun.*, 2018, **54**, 8269–8272.

61 Y.-X. Han, C.-L. Hu, B.-X. Li and J.-G. Mao, $LnLiSiS_4$ (Ln = La and Ce): Promising infrared nonlinear optical materials designed by aliovalent substitution from $SrCdSiS_4$, *Mater. Today Phys.*, 2023, **31**, 100987.

62 Y. Zhang, J. Chen, K. Li, H. Wu, Z. Hu, J. Wang, Y. Wu and H. Yu, $LaMg_6Ga_6S_{16}$: a chemical stable divalent lanthanide chalcogenide, *Nat. Commun.*, 2024, **15**, 2959.

63 G. Li, Z. Yang and S. Pan, $LiAlS_2$: A promising infrared frequency-conversion material with ultrawide band gap and high laser-induced damage threshold, *Sci. China Mater.*, 2023, **66**, 1189–1196.

64 M. Sun and J. Yao, Ba_2HgTe_5: a Hg-based telluride with giant birefringence induced by linear $[HgTe_2]$ units, *Inorg. Chem. Front.*, 2022, **9**, 5024–5031.

65 M. Sun, X. Zhang, W. Xing, E. Uykur, W. Yin, Z. Lin and J. Yao, $Ba_6In_2Ge_2Te_{15}$: a THz birefringent material with an intriguing quasi-$[Te_5]^{4-}$ chain possessing large optical anisotropy and an ultrawide transmission range, *Inorg. Chem. Front.*, 2022, **9**, 3421–3427.

66 X. Huang, S.-H. Yang, W. Liu and S.-P. Guo, Noncentrosymmetric $Ba_6In_2Q_{10}$ (Q = S, Se): Structural

Chemistry and Nonlinear-Optical Activity, *Inorg. Chem.*, 2021, **60**, 16932–16936.

67 K. Wu, Z. Yang and S. Pan, Na_2BaMQ_4 (M=Ge, Sn; Q=S, Se): Infrared Nonlinear Optical Materials with Excellent Performances and that Undergo Structural Transformations, *Angew. Chem., Int. Ed.*, 2016, **55**, 6713–6715.

68 K. Wu, B. Zhang, Z. Yang and S. Pan, New Compressed Chalcopyrite-like $Li_2BaMIVQ_4$ (MIV = Ge, Sn; Q = S, Se): Promising Infrared Nonlinear Optical Materials, *J. Am. Chem. Soc.*, 2017, **139**, 14885–14888.

69 B. Krebs, Thio- and Selenoborates: from Rings to Clusters and Networks, *Phosphorus, Sulfur Silicon Relat. Elem.*, 2001, **168**, 11–22.

70 B. Krebs and W. Hamann, Ortho-thioborates and ortho-selenoborates: synthesis, structure and properties of Tl_3BS_3 and Tl_3BSe_3, *J. Less-Common Met.*, 1988, **137**, 143–154.

71 A. Hammerschmidt, C. Köster, J. Küper, A. Lindemann and B. Krebs, Novel Alkaline Earth Metal Chalcogenoborates: Syntheses and Crystal Structures of $Sr_{4.2}Ba_{2.8}(BS_3)_4S$ and $Ba_7(BSe_3)_4Se$, *Z. Anorg. Allg. Chem.*, 2001, **627**, 1253–1258.

72 M. Döch, A. Hammerschmidt, S. Pütz and B. Krebs, ISOLATED $B_{10}Se_{20}$-MACROTETRAHEDRA IN THE NOVEL QUATERNARY SELENOBORATE $Li_{6-2x}Sr_{2\ +x}B_{10}Se_{20}$ ($x \approx 0.7$), *Phosphorus, Sulfur Silicon Relat. Elem.*, 2004, **179**, 933–935.

73 Y.-Y. Li, B.-X. Li, G. Zhang, L.-J. Zhou, H. Lin, J.-N. Shen, C.-Y. Zhang, L. Chen and L.-M. Wu, Syntheses, Characterization, and Optical Properties of Centrosymmetric $Ba_3(BS_3)_{1.5}(MS_3)_{0.5}$ and Noncentrosymmetric $Ba_3(BQ_3)(SbQ_3)$, *Inorg. Chem.*, 2015, **54**, 4761–4767.

74 A. Lindemann, J. Küper, W. Hamann, J. Kuchinke, C. Köster and B. Krebs, Syntheses, Crystal Structures, and Properties of the Three Novel Perselenoborates $RbBSe_3$, $CsBSe_3$, and $TlBSe_3$ with Polymeric Chain Anions, *J. Solid State Chem.*, 2001, **157**, 206–212.

75 A. Hammerschmidt, J. Küper, L. Stork and B. Krebs, $Na_2B_2Se_7$, $K_2B_2S_7$ und $K_2B_2Se_7$: Drei Perchalkogenoborate mit neuem polymeren Anionengerüst, *Z. Anorg. Allg. Chem.*, 1994, **620**, 1898–1904.

76 A. Lindemann, J. Küper, C. Jansen, J. Kuchinke, C. Köster, A. Hammerschmidt, M. Döch, T. Pruß and B. Krebs, Syntheses and Crystal Structures of $Rb_2B_2Se_7$, $Tl_2B_2Se_7$, $Cs_3B_3Se_{10}$, and $Tl_3B_3Se_{10}$: New Perseleno-selenoborates with Polymeric Anionic Chains, *Z. Anorg. Allg. Chem.*, 2001, **627**, 419–425.

77 A. Hammerschmidt, A. Lindemann, M. Döch, C. Köster and B. Krebs, 2D-Polymeric Anion Networks: The Two Novel Perselenoborates BaB_2Se_6 and $Ba_2B_4Se_{13}$, *Z. Anorg. Allg. Chem.*, 2002, **628**, 1561–1567.

78 J. Kuchinke, A. Lindemann, C. Köster, A. Hammerschmidt, M. Döch, T. Pruss and B. Krebs, $Li_{6(-x}Cs_xB_{10}Q_{18}$ (Q = S, Se; $x \sim 1$): New Polymeric Layered Anion Networks in Chalcogenoborates, *Phosphorus, Sulfur Silicon Relat. Elem.*, 2001, **169**, 281–284.

79 S. Bagci, B. G. Yalcin, H. A. R. Aliabad, S. Duman and B. Salmankurt, Structural, electronic, optical, vibrational and transport properties of $CuBX_2$ (X = S, Se, Te) chalcopyrites, *RSC Adv.*, 2016, **6**, 59527–59540.

80 L.-J. Chen, J.-D. Liao, Y.-J. Chuang and Y.-S. Fu, Synthesis and Characterization of $Cu(In_xB_{1-x})Se_2$ Nanocrystals for Low-Cost Thin Film Photovoltaics, *J. Am. Chem. Soc.*, 2011, **133**, 3704–3707.

81 A. Lindemann, J. Kuchinke, C. Köster, A. Hammerschmidt, M. Döch, T. Pruss and B. Krebs, The First Perselenoborate with a Novel Three-Dimensional Anion Network, *Phosphorus, Sulfur Silicon Relat. Elem.*, 2001, **169**, 169–172.

82 S. Pütz, M. Döch, A. Hammerschmidt, A. Lindemann, H. Eckert, T. Nilges and B. Krebs, $Li_7B_7Se_{15}$: A novel selenoborate with a zeolite-like polymeric anion structure, *Solid State Sci.*, 2006, **8**, 764–772.

83 A. Hammerschmidt, A. Lindemann, M. Döch and B. Krebs, $Na_6B_{10}Se_{18}$: a novel selenoborate with a 3D polymeric anion structure, *Solid State Sci.*, 2002, **4**, 1449–1455.

84 A. Hammerschmidt, M. Döch, S. Pütz, H. Eckert and B. Krebs, $Li_{6+2x}[B_{10}Se_{18}]Se_x$ ($x \approx 2$), ein ionenleitendes Doppelsalz, *Z. Anorg. Allg. Chem.*, 2006, **632**, 1219–1226.

85 J. Küper, O. Conrad and B. J. A. C. Krebs, Selenoboratoborate $[B_{12}(BSe_3)_6]^{8-}$: eine neue Klasse chalkogensubstituierter ikosaedrischer Borcluster, *Angew. Chem., Int. Ed.*, 1997, **109**, 1995–1996.

86 A. Lindemann, J. Kuchinke and B. Krebs, Drei neue Selenoborato-closo-dodekaborate: Synthesen und Kristallstrukturen von $Rb_8[B_{12}(BSe_3)_6]$, $Rb_4Hg_2[B_{12}(BSe_3)_6]$ und $Cs_4Hg_2[B_{12}(BSe_{3)6}]$, *Z. Anorg. Allg. Chem.*, 1999, **625**, 1165–1171.

87 A. Hammerschmidt, A. Lindemann, C. Köster and B. Krebs, $Na_6[B_{18}Se_{17}]$: The First Selenoborato-closo-dodecaborate with a Polymeric Chain Anion, *Z. Anorg. Allg. Chem.*, 2001, **627**, 2121–2126.

88 A. Hammerschmidt, A. Lindemann, M. Döch and B. Krebs, $K_8[B_{12}(BSe_3)_6]$: A Novel Selenoborato-closo-dodecaborate with Different Anion Substitution Patterns, *Z. Anorg. Allg. Chem.*, 2003, **629**, 1249–1255.

89 A. Hammerschmidt, M. Döch, S. Pütz and B. Krebs, $Na_8[B_{12}(BSe_3)_6]$: A Novel Selenoborato-closo-dodecaborate, *Z. Anorg. Allg. Chem.*, 2004, **630**, 2299–2303.

90 A. Hammerschmidt, M. Döch, S. Pütz and B. Krebs, $Na_2[B_{18}Se_{16}]$: The First 3D Polymeric Selenoborato-closo-dodecaborate, *Z. Anorg. Allg. Chem.*, 2005, **631**, 1125–1128.